$K\alpha$ satellite and hypersatellite distributions of Ar excited in heavy-ion collisions

V. Horvat,[*] R. L. Watson, and Y. Peng

Cyclotron Institute and Department of Chemistry, Texas A&M University, College Station, Texas 77843-3366, USA

Spectra of $K\alpha$ x rays emitted from Ar gas at atmospheric pressure under bombardment by 10 MeV/amu heavy ions (atomic number 6–79) were measured in high resolution using a curved crystal spectrometer. Values of the apparent average fraction of L vacancies at the time of $K\alpha$ x-ray emission (p_L^x) were determined from the observed $K\alpha$ satellite and hypersatellite intensity distributions. A systematic comparison of the p_L^x values for the monatomic gas Ar with those obtained previously for a variety of solid targets provided a quantitative assessment of the role interatomic transitions play in the L-vacancy transfer process that occurs prior to K x-ray decay.

I. INTRODUCTION

Over the years, a number of investigations of the $K\alpha$ x-ray satellite structure produced by heavy-ion bombardment of low to intermediate atomic number targets have shown that the L-vacancy distribution is sensitive to the physical and chemical environment [1–6]. These measurements have revealed that the apparent degree of L-shell ionization (as reflected by the relative intensities of the $K\alpha$ satellites) decreases as the average valence electron density increases. Furthermore, it has been found that the apparent degrees of L-shell ionization produced in gaseous hydrides (e.g., SiH_4, H_2S, and HCl) are much higher than those observed for the corresponding elements in the solid state [3,4,6]. These effects have been attributed to L-vacancy transfer processes that alter the original L-vacancy distribution (created in the heavy-ion collision) prior to $K\alpha$ x-ray decay. One obvious mechanism for L-vacancy transfer involves intra-atomic (x-ray and Auger) transitions to higher shells. However, rationalization of the gas vs solid differences mentioned above requires an additional mechanism involving transitions from neighboring atoms (i.e., interatomic transitions). Since these early studies were conducted, very little progress has been made in quantifying the contributions of intra- and inter-atomic transitions to the L-vacancy transfer process.

Recently, we have measured the spectra of $K\alpha$ satellite x rays from a variety of solid targets under bombardment by heavy ions using a crystal spectrometer [7]. The targets contained elements having atomic numbers ranging from 17 (Cl) to 32 (Ge), while the projectiles ranged in atomic number from 6 (C) to 83 (Bi) and in energy from 2.5 to 25 MeV/amu. This comprehensive set of measurements revealed that the experimentally determined parameter p_L^x (the apparent average fraction of L vacancies at the time of $K\alpha$ satellite x-ray emission) defines a universal curve when plotted as a function of a (universal) variable X_2, whose value is determined in a unique way by the collision parameters (i.e., projectile atomic number, projectile energy, and target atomic number) [7]. This finding provides a basis for comparison of the p_L^x values for different collision systems (i.e.,

without restricting it to those with almost identical collision parameters). Additionally, it provides the means to quantitatively describe the systematic effects of different physical and chemical environments of target atoms on the p_L^x values.

The objective of the present work is to assess the effect of interatomic transitions on the L-vacancy transfer process and to investigate its dependence on collision parameters. This was accomplished by delineating the dependence of p_L^x on the universal variable for a monatomic gas (argon) and comparing the result to the curve obtained previously [7] for solid targets. Since the average separation between atoms of a monatomic gas is large, interatomic transitions in an Ar target are effectively absent, so that the difference between the two curves mentioned above provides a direct quantitative measure of the contribution of interatomic transitions to the target L-vacancy transfer that occurs between the time of collision and the time of $K\alpha$ x-ray emission.

II. EXPERIMENT

Beams of 10 MeV/amu C, Ne, S, Fe, Kr, Xe, Ho, Ta, and Au were delivered from the Texas A&M K-500 superconducting cyclotron. The beams were aligned and focused with the aid of a closed-circuit television camera and a Zn/CdS phosphor positioned at the location designated for the target gas cell center. During the measurements, the beams were collimated to a diameter of 2 mm before passing through the gas cell and on to a copper beam stop. Radiation from the beam stop was detected by a plastic scintillation detector and used to monitor the beam intensity.

The beam entrance and exit apertures of the gas cell were sealed from the vacuum system by means of 2.1 mg/cm^2 nickel foils. The distance between the entrance and exit apertures was 1.5 cm and the x rays were viewed by the spectrometer through a 540 μg/cm^2 mylar window located at the top of the cell. A collimator placed over the x-ray window restricted the observed projectile path length to 0.33 cm. A constant pressure of 1 atm (10^5 Pa) inside the gas cell was maintained by a slow continuous flow of Ar gas from a pressurized bottle into the atmosphere.

Ar target K x rays were measured in high resolution using a 12.7 cm Johansson-type curved crystal spectrometer equipped with a LiF(200) crystal. The spectra were measured
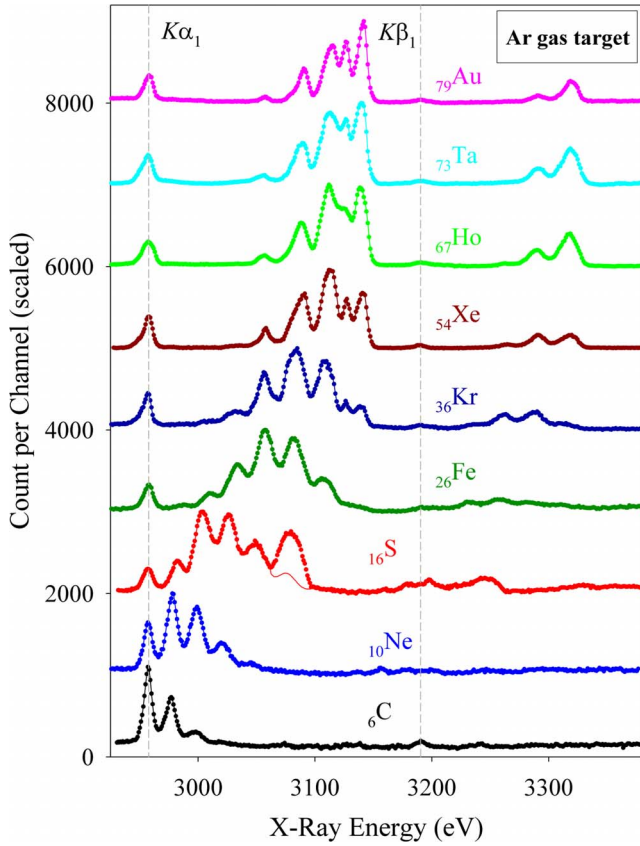
─────────
*V-Horvat@tamu.edu

FIG. 1. (Color online) Measured spectra of x rays emitted from Ar gas at a pressure of 1 atm under bombardment by 10 MeV/amu ions (as labeled). Positions of the $K\alpha_1$ and $K\beta_1$ diagram transitions are indicated by the vertical dashed lines. The solid circles show the raw spectra, while the solid lines simply connect the data points. One exception is the spectrum obtained with sulfur projectiles, where the line shows the corrected spectrum after subtraction of estimated contributions of sulfur x rays due to $M \rightarrow K$ transitions.

in the first order of diffraction with the spectrometer focal circle oriented at 90° relative to the beam direction. Diffracted x rays were detected by a proportional counter filled with P-10 gas (90% Ar and 10% CH_4) flowing at atmospheric pressure.

Energy calibration of the measured spectra was based on peaks that are mainly due to Ar $K\alpha_{1,2}$ and $K\beta_{1,3}$ diagram transitions. Energies of these transitions were taken from Ref. [8]. The resolution of the spectrometer (full width at half maximum) was found to be 7.3 eV, as determined in a least-squares fit of a Voigt function to the Ar $K\alpha_{1,2}$ diagram peak profile using the literature value of 7.9 eV for the Lorentzian component width [9].

III. DATA ANALYSIS

Normalized spectra of Ar $K\alpha$ x rays recorded in the present work are shown in Fig. 1. The positions of the $K\alpha_1$ and $K\beta_1$ diagram transitions are indicated by the vertical dashed lines. The peak at the $K\alpha_1$ diagram transition line includes unresolved contributions from $2p \rightarrow 1s$ transitions in target atoms with a single vacancy and in target atoms with

additional M vacancies. The former are known as $K\alpha$ diagram transitions, while the latter will be referred to as $K\alpha L^0$ satellite transitions. Additional spectator vacancies in the L shell give rise to the peaks that are shifted higher in energy. In the present case, peaks corresponding to different numbers (i) of L vacancies are resolved from each other. They will be referred to as $K\alpha L^i$ satellites. The $K\alpha L^i$ satellite transitions ($i = 0$–7) are almost exclusively due to K-vacancy production by heavy-ion projectiles, while the diagram transitions are typically due to secondary K-shell ionization [10,11]. As expected from previous work, Fig. 1 shows that the distribution of $K\alpha$ satellites shifts to higher average values of i with increasing projectile atomic number.

The M-vacancy distribution associated with $K\alpha L^i$ satellite transitions affects the widths and centroids of the corresponding peaks. Typically, this effect is small enough that the $K\alpha L^i$ satellites still can be resolved from each other, but large enough to obliterate any structure that might arise due to the various ways in which the electronic angular momenta can be coupled (i.e., multiplet splitting), although, in most cases, such structure cannot be observed due to the complexity of multiplet splitting alone. However, there are two notable exceptions. One corresponds to the case in which $i=0$ and the average number of M vacancies is much less than one, while the other corresponds to the case in which $i=7$ and the average number of M vacancies is very close to the maximum (i.e., 8 for Ar). In the former case it may be possible to resolve the $K\alpha_{1,2}$ doublet provided that the resolution of the spectrometer is adequate (which is not the case here), while in the latter case it may be possible to resolve the two major components of the $K\alpha L^7$ satellite (which was accomplished in the present work).

Figure 1 shows that the two $K\alpha L^7$ peak components were resolved in the spectra induced by Kr, Xe, Ho, Ta, and Au projectiles. In the absence of M electrons, the peak component at a lower energy corresponds to the $1s2p(^3P) \rightarrow 1s^2(^1S)$ transition, while the other at a higher energy corresponds to the $1s2p(^1P) \rightarrow 1s^2(^1S)$ transition. The predominant contribution to the ^3P peak is expected to originate from the $^3P_1$ state, which should be formed with the same statistical probability as the $^1P_1$ state, but its decay is delayed because $^3P \rightarrow ^1S$ transitions are spin forbidden. Therefore, there is a significant probability that the ^3P state will decay by nonradiative means, such as collisional quenching (see Ref. [12], and references therein), which leads to a reduction in the intensity of the $^3P \rightarrow ^1S$ peak relative to the $^1P \rightarrow ^1S$ peak.

A spectator vacancy in the K shell gives rise to peaks that are shifted even higher in energy. They are referred to as $K^2\alpha L^i$ satellites or $K\alpha$ hypersatellites. In the case of Ar, the $K^2\alpha L^0$ satellite lies at 3131 eV [13], between the $K\alpha L^7$ satellite and the $K\beta_{1,3}$ diagram peak, but only those $K\alpha$ hypersatellites that lie above the $K\beta_{1,3}$ diagram peak were observed in the present measurements. As illustrated in Fig. 1, the $K\alpha$ hypersatellite distribution also shifts to higher average values of i with increasing projectile atomic number. For Ar bombarded by 10 MeV/amu projectiles, the intensity of the hypersatellites relative to the satellites reaches a maximum around $Z_1 = 73$. In the spectra induced by C and Ne projectiles, the $K\alpha$ hypersatellites are buried in the back-
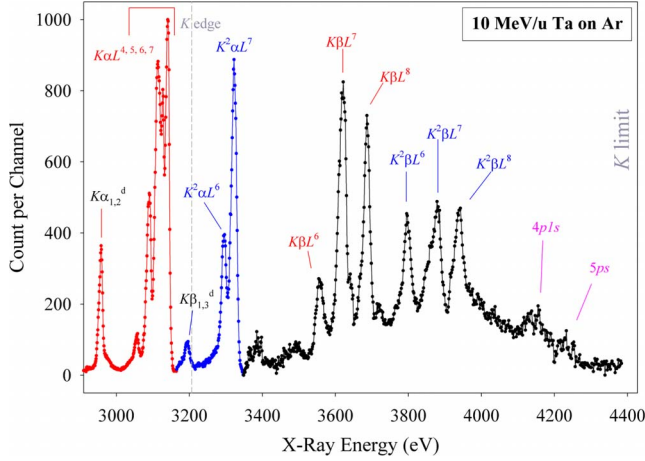
FIG. 2. (Color online) Measured spectrum of Ar K x rays induced by 10 MeV/amu Ta projectiles. For x-ray energies from 3165 to 3347 eV and from 3348 to 4384 eV, the number of counts per channel has been multiplied by factors of 2 and 4, respectively.

ground and, consequently, they were not analyzed.

The measured x-ray spectrum induced by sulfur ions contains significant contributions from projectile $K\beta$ transitions. Since 10 MeV/amu S ions are expected to be almost fully stripped while they are inside the gas cell [14], these transitions should be mostly hydrogenlike (Lyman type). However, the peak due to these transitions is somewhat shifted down in energy due to the Doppler effect and it overlaps with the Ar $K\alpha L^5$ satellite. The red data points in Fig. 1 show the uncorrected (normalized) spectrum, while the red line shows the same spectrum after subtraction of the sulfur peak. Small peaks due to sulfur $np \rightarrow 1s$ transitions $(n > 3)$ can be seen in the $K\alpha$ hypersatellite region. Iron projectile $K\alpha$ x rays diffracted in second order also may contribute to the Ar x-ray spectrum in the $K\alpha$ hypersatellite region. Although this is not obvious in Fig. 1, it became apparent upon analysis of the spectrum. Therefore, the presentation of results for the Ar $K\alpha$ hypersatellite distributions will be limited to those obtained from the spectra excited by Kr, Xe, Ho, Ta, and Au projectiles.

A complete spectrum of Ar K x rays excited by 10 MeV/amu Ta projectiles is shown in Fig. 2. In addition to the $K\alpha$ satellites and $K\alpha$ hypersatellites, it also features the $K\beta$ satellites and $K\beta$ hypersatellites as well as structures due to Ar $4p \rightarrow 1s$ and $5p \rightarrow 1s$ transitions. The major peaks were identified by comparing their measured energies with those predicted by Dirac-Fock calculations [15].

The intensity distributions of the K satellites and hypersatellites may be characterized quantitatively in terms of the apparent average fraction of L vacancies at the time of K x-ray emission (p_L^x), defined as

$$p_L^x = \frac{1}{8} \sum_{i=1}^{8} (i I_i) / I_{tot},\qquad (1)$$

where

$$I_{tot} = \sum_{i=0}^{8} I_i.\qquad (2)$$

In this work, p_L^x was determined using Eqs. (1) and (2) in which I_i were the intensities of the $K\alpha L^i$ or $K^2\alpha L^i$ peaks. Although, in principle, p_L^x also can be determined from the intensities of the $K\beta$ satellites or $K\beta$ hypersatellites, this was not done here because these peaks are less intense, more spread out, and the two groups overlap (see Fig. 2). Consequently, it would take considerably more data acquisition time to obtain adequate counting statistics, the data analysis would be much more complicated, and the results would be more uncertain. Bearing this in mind, the spectra of $K\beta$ satellites and $K\beta$ hypersatellites were recorded only in runs with Ta projectiles (shown in Fig. 2) and Ho projectiles (not shown). However, it is worth pointing out that the p_L^x values for the $K\beta$ satellites and hypersatellites are generally larger than those for the $K\alpha$ satellites and hypersatellites because I_8 can make a significant contribution to the former (see Fig. 2), while I_8 is zero for the latter. Namely, with eight vacancies in the L shell, there are no L electrons left to make a $K\alpha$ (i.e., $2p \rightarrow 1s$) transition. However, since p_L^x is defined here as the *apparent* average fraction of L vacancies, and in order to preserve consistency with previous results (in which this effect was much smaller) [7], no correction for this effect was attempted. The potential impact of such a correction is discussed in Sec. IV.

In the analysis of the spectra, the majority of x-ray peaks were fit with single Voigt functions, but some required two or more in order to reproduce their shapes accurately. The width of the Lorentzian component was fixed at 7.9 eV [9]. Two examples of fitted $K\alpha$ satellite spectra (excited with Au and Fe projectiles) are shown in Fig. 3. The measured data points are shown as solid black circles, while the thick solid (red) line represents the overall fit. The background is shown as a thick dashed (gray) line, while the thin solid (green) line outlines the contributions from the diagram x rays. The thin dashed (blue) lines represent the combined contributions from all the Voigt functions that were used to fit an individual peak.

In the spectrum excited by sulfur projectiles, the intensity of the $K\alpha L^5$ satellite was estimated by fitting a binomial distribution to the measured intensities of the $K\alpha L^2$, $K\alpha L^3$, and $K\alpha L^4$ satellites and using the predicted binomial intensity for $K\alpha L^5$ along with the profile of the $K\alpha L^4$ peak to construct the $K\alpha L^5$ satellite, as shown by the solid red line in Fig. 1. The corrected spectrum was then reanalyzed.

A similar procedure was used to estimate the intensity of the (collision-excited) $K\alpha L^0$ satellite in the spectra induced by Ne, S, and Fe projectiles. The remainder of the peak observed at that position was attributed to diagram x rays induced by secondary radiation (x rays and electrons). That contribution was found to be 16%, 83%, and 97%, respectively, of the total number of counts in the observed peak and its effect on the calculated value of p_L^x was 3%, 4%, and 0.2% compared to the value of p_L^x obtained assuming contributions of 0%, 0%, and 100%. The contribution from secondary radiation was assumed to be negligible for the spec-
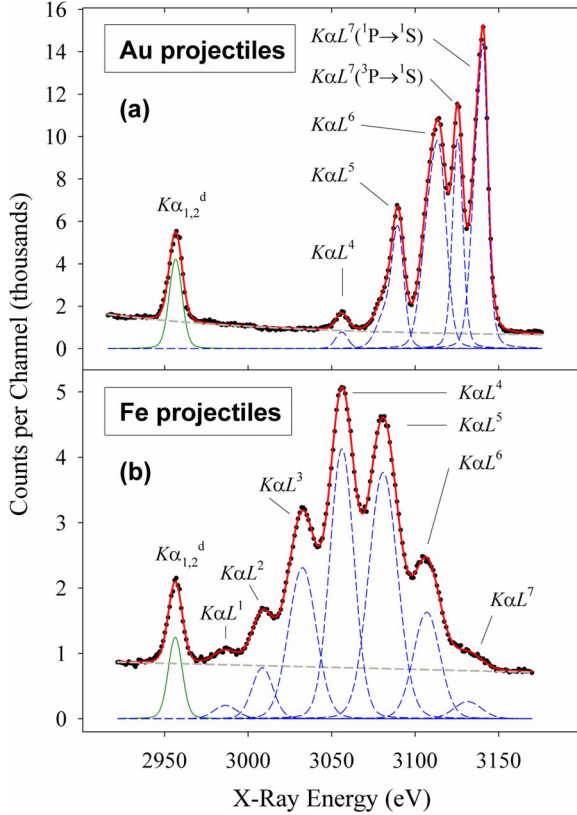
FIG. 3. (Color online) Fitted $K\alpha$ satellite spectra of Ar induced by (a) Au and (b) Fe projectiles at 10 MeV/amu. The measured data points are shown as solid black circles, while the thick solid (red) line represents the overall fit. The background is shown as a thick dashed (gray) line, while the thin solid (green) line outlines the contributions from the diagram x rays. The thin dashed (blue) lines represent the individual satellites or their major components (as labeled).

trum excited by C projectiles and equal to 100% of the observed peak for the spectra induced by Kr, Xe, Ho, Ta, and Au projectiles.

For consistency with previous results [7], the relative peak intensities were not corrected for absorption and spectrometer efficiency. These corrections were found to be small [16] and in the present case they are also counteracting, since 90% of the gas in the proportional counter is the same as the target gas, so that an x ray that is absorbed more in the target gas is also detected by the proportional counter with higher efficiency.

IV. RESULTS AND DISCUSSION

Multiple ionization of an atomic shell characterized by its principal quantum number n under bombardment by heavy ions can be described in terms of the geometrical model [17]. The model predicts that the n-shell ionization probability per electron (p_n) is a function of a universal variable (X_n),

$$X_n = 4V[G(V)]^{1/2}Z_1\alpha c/(nv_1). \tag{3}$$

In the expression above, Z_1 and v_1 are the projectile atomic number and speed, α is the fine structure constant, c

is the speed of light in vacuum, $V = v_1/v_2$, where v_2 is the average speed of an electron having principal quantum number n, and $G(V)$ is the binary encounter approximation scaling function [18]. According to the geometrical model, the average fraction of n-shell vacancies can be well approximated by the simple expression [17]

$$p_n = X_n^2/\{4.2624 + X_n^2[1 + 0.5 \exp(-X_n^2/16)]\}. \tag{4}$$

Since the atomic relaxation does not depend on the source of excitation, it was expected that p_L^x retains the universal scaling properties of p_L (i.e., p_n for $n=2$). Indeed, it has been established [7] that the experimentally determined values of p_L^x do define a universal curve when plotted as a function of X_2. This universal curve was found to be well described by a logistic function of the form

$$p_L^x = a/[1 + (b/X_2)^c]. \tag{5}$$

Such a function has a sigmoidal shape, equals zero at $X_2 = 0$, and its asymptotic (maximum) value is a. The parameter b represents the value of the universal variable at which the function reaches one half of its asymptotic value, while the parameter c is proportional to the slope of the curve at $X_2 = b$. Based on 128 different spectra of $K\alpha$ x rays, the best-fit values of the parameters were found to be $a = 0.537 \pm 0.006$, $b = 2.11 \pm 0.08$, and $c = 2.02 \pm 0.03$ [7].

Introduction of the universal variable greatly simplifies comparisons between experimental results obtained under various conditions. Furthermore, the results described above provide a means of accurately predicting the values of p_L^x in collision systems (within the same regime) for which the experimental results are not available. With regard to comparison of the experimental results for solid targets with the predictions of the geometrical model [Eq. (4)], however, large discrepancies were found [7]. These discrepancies monotonically increase as the value of the universal variable increases, and the asymptotic value of p_L is almost twice the asymptotic value of p_L^x. Such large discrepancies cannot be accounted for by postcollision intra-atomic vacancy rearrangement alone [19]. This suggests that interatomic transitions may play a substantial role in reducing the value of p_L^x for atoms in a solid-state environment relative to the value of p_L predicted by the geometrical model.

Table I presents a list of projectile ions used in this work along with their estimated average kinetic energies at the center of the gas cell and the corresponding values of the geometrical model's universal variable [Eq. (3)]. The last two columns in Table I show the values of p_L^x determined using Eqs. (1) and (2) from the intensities of Ar $K\alpha$ satellites and hypersatellites obtained by least-squares curve fitting of the spectra. They are also plotted in Fig. 4 as a function of the universal variable, where the open circles show the results for the $K\alpha$ satellites and the filled circles show the results for the $K\alpha$ hypersatellites. The thin solid (red) line is the best-fit logistic curve for the satellite data points, while the thin dashed (green) line is the best-fit logistic curve for the hypersatellite data points. The thick solid (blue) line is the best-fit logistic curve for p_L^x values obtained from $K\alpha$ satellites in the measurements with various *solid* targets (atomic numbers $Z_2 = 17-32$) [7]. The thick dashed (black)

TABLE I. Atomic numbers (Z_1) of projectiles used in this work and their estimated average kinetic energies at the center of the gas cell filled with argon gas at atmospheric pressure. Also listed are the corresponding values of the geometrical model's universal variable X_2 and the corresponding measured values of the apparent average fraction of L vacancies at the time of K x-ray emission as determined from the intensities of Ar $K\alpha$ satellites [$p_L^x(K\alpha^s)$] and Ar $K\alpha$ hypersatellites [$p_L^x(K\alpha^h)$] using Eqs. (1) and (2). The numbers in parentheses represent the errors in the last digit(s) of the p_L^x values. The errors were derived from the uncertainties in the best-fit values of the peak intensities.

Z_1	E (MeV/amu)	X_2^a	$p_L^x(K\alpha^s)$	$p_L^x(K\alpha^h)$
6	9.6	0.893	0.089 (1)	
10	9.4	1.50	0.210 (1)	
16	9.1	2.43	0.363 (1)	
26	8.8	4.01	0.537 (1)	0.626 (1)
36	8.7	5.58	0.637 (1)	0.691 (3)
54	8.6	8.40	0.731 (1)	0.789 (1)
67	8.5	10.5	0.770 (2)	0.822 (1)
73	8.5	11.4	0.779 (12)	0.814 (1)
79	8.5	12.3	0.790 (3)	0.829 (1)

^{a}The value of X_2 was calculated using the BEA scaling function of Gryzinski [18], while ν_2 was derived from the neutral atom binding energy of L_3 electrons [8].

line represents the predicted values of p_L, the average fraction of L vacancies produced in heavy-ion collisions at small impact parameters, according to the geometrical model [Eq. (4)].

It is evident that the measured values of p_L^x for the Ar $K\alpha$ satellites and for the Ar $K\alpha$ hypersatellites are well represented by logistics curves when plotted as a function of the universal variable. This finding, together with the previous results for solid targets, emphasizes the important role the universal variable plays in delineating the systematic behavior of multiple vacancy production in heavy-ion collisions.

The average scatter of the nine $_{18}$Ar satellite data points, as measured by the rms deviation from the best-fit curve (0.0044 or 3.4%), is comparable to that found previously [7] for $_{17}$Cl (0.0057 or 1.2%) and $_{19}$K (0.0077 or 2.0%) in a solid KCl target (9 points each), but significantly smaller than the overall average scatter of the entire set of 128 data points for solid targets (0.019 or 5.8%). Furthermore, the extent of the overall rms deviation is in agreement with the range of p_L^x values found previously for compounds containing third-row elements in measurements with the 2 MeV/amu oxygen ions (0.012 for Al, 0.033 for Si, 0.052 for S, and 0.018 for Cl) [5]. The same holds for the more recent results from measurements involving various compounds of tin [7] and vanadium [20]. This suggests that the overall scatter in the solid target data of up to about 0.02 units is mainly due to effects of chemical environment and to a lesser extent due to experimental uncertainties.

Comparison of the satellite curve for Ar gas (best-fit parameters $a = 0.856 \pm 0.007$, $b = 2.94 \pm 0.05$, and $c = 1.71 \pm 0.04$) with that for solid targets (best-fit parameters $a = 0.537 \pm 0.006$, $b = 2.11 \pm 0.08$, and $c = 2.02 \pm 0.03$) [7]
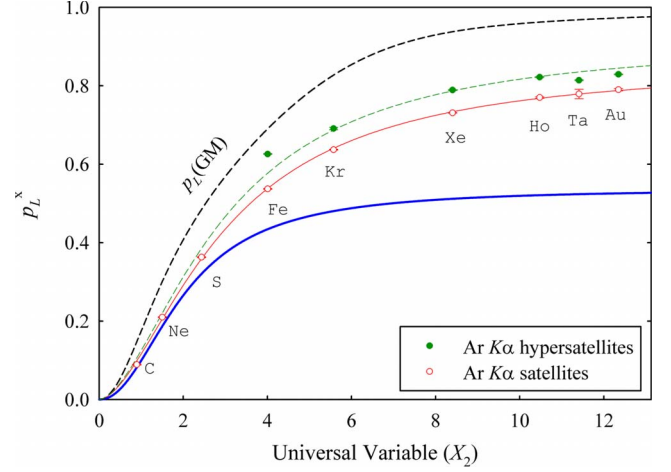

FIG. 4. (Color online) The apparent average fraction of L vacancies at the time of $K\alpha$ x-ray emission (p_L^x) as a function of the universal variable X_2. The hollow (red) and solid (green) circles represent $p_L^x(K\alpha^s)$ and $p_L^x(K\alpha^h)$] from Table I. The thin solid (red) line and the thin dashed (green) line show the corresponding best-fit logistic curves. The thick dashed line shows the geometrical model's prediction of p_L [Eq. (4)], the average fraction of L vacancies produced in the collisions, while the thick solid (blue) line represents the best-fit logistic curve for p_L^x values from $K\alpha$ satellites in measurements with solid targets (from Ref. [7]).

shows that the former curve is always above the latter. They lie close to each other (within 0.02 units) for $X_2 < 1.7$, but as X_2 increases beyond the value of 1.7, the gap between the two curves keeps increasing. The curve for solid targets reaches 90% of its asymptotic value around $X_2 \approx 5.7$, while the curve for Ar gas reaches 90% of its asymptotic value at a much larger value of X_2 (i.e., at $X_2 \approx 10.6$). Furthermore, the asymptotic value of the curve for Ar gas is found to be as much as 60% higher than the one for solid targets.

The striking difference between the two curves is presumably due to interatomic transitions that occur in a solid-state environment, but are effectively absent in a monatomic gas. Apparently, interatomic electron transfer plays a very substantial role in reducing the number of L vacancies present at the time of K x-ray emission at large values of X_2 (i.e., for atoms that have lost a large number of L electrons in a collision with a heavy ion).

It is expected that a highly ionized atom in a solid target eventually becomes neutralized and reaches its ground-state configuration. In the process, the missing electrons must be supplied from the atom's environment. What may be surprising is that such a significant portion of this process occurs prior to $K\alpha$ x-ray emission, resulting in a reduction of the p_L^x value by as much as 40% (0.319 units) compared to the value of p_L^x in a monatomic gas at the same value of X_2. Since interatomic electron transfer is not available to atoms in monatomic gases, they retain a much higher degree of L-shell ionization at the time of $K\alpha$ x-ray emission compared to atoms in the solid state.

Figure 4 also suggests that as the value of X_2 decreases, the effects of interatomic transitions on the spectra of $K\alpha$ x rays become less important. This is a consequence of the increased availability of outer-shell electrons for intra-atomic

transitions as well as the reduced availability of L and higher-shell vacancies to accommodate interatomic electron transfer. Although previous observations of x-ray satellite distributions for monatomic gases generally have shown them to exhibit higher p_L^x values than those for the neighboring elements in solids (see Ref. [6], and references therein), the present method of comparison provides a more systematic and quantitative means of evaluation.

In the absence of interatomic transitions, the value of p_L^x is expected to be somewhat larger in solid targets than in monatomic gases for a given value of X_2. This is because projectiles traveling in solids have more inner-shell vacancies and higher charges, on average, than those traveling in gases due to the fact that the time between successive collisions in solids is shorter than typical excited-state lifetimes. Such projectiles are more likely to capture target L electrons in K-shell ionizing collisions. The cross sections for direct ionization are also expected to be larger due to reduced electron screening of the projectile nucleus. Both processes result in higher p_L^x values. Consequently, the effect of interatomic transitions on the value of p_L^x for atoms in solids is expected to be even larger than is implied by the difference between the two empirical p_L^x curves.

Presumably, diatomic gas molecules should exhibit a behavior that is intermediate between that of a solid and a monatomic gas. This expectation was tentatively confirmed in a preliminary measurement with a Cl_2 target (also at the atmospheric pressure) excited by 6 MeV/amu Xe projectiles. After passing through the Ni window and reaching the center of the gas cell, the projectile energy was reduced to 3.7 MeV/amu yielding an X_2 value of 11.5. The measured $K\alpha$ x-ray spectrum is shown in Fig. 5 of Ref. [7]. Its p_L^x value was determined to be 0.69, which is well below the value of 0.779 obtained for Ar at a similar value of X_2 (see the entry for Ta projectiles in Table I), and well above the value of 0.521 predicted for a solid target using Eq. (5). Apparently, the value of p_L^x is a sensitive indicator of the relative importance of interatomic collisions, especially at large values of X_2. The result for Cl_2 gas also shows that the effect of interatomic transitions can be quite large even if there is only one neighboring atom present, despite the possibility that, under favorable orientation of the Cl_2 molecule at the time of collision, the other Cl atom may be highly ionized as well. Also, the time available for interatomic transitions is ultimately limited due to Coulomb dissociation of the molecular ion created in the collision with a heavy ion.

Due to low counting statistics and high background, reliable values of p_L^x for the $K\alpha$ hypersatellite intensity distributions could not be obtained for measurements with projectiles lighter than Kr. Nevertheless, the data point for Fe projectiles is listed in Table I and plotted in Fig. 4, but it was not used in the regression analysis. Due to the lack of data points at low values of X_2, the parameters b and c of the best-fit logistic curve could not be determined accurately. Therefore, their values were assumed to be the same as the respective values obtained from the analysis of the satellites (i.e., $b=2.94$, $c=1.71$), while the remaining parameter (a) was varied. The best-fit value of a was found to be 0.909 ± 0.006.

This asymptotic value of p_L^x is close to the asymptotic value $p_L=1$ predicted by the geometrical model. However, the best-fit logistic curve is still very different from the geometrical model curve. Nevertheless, the differences between the two curves are not excessive and it might be possible to explain them based on intra-atomic postcollision vacancy rearrangement alone. The same might be true for the curve obtained from Ar $K\alpha$ satellites.

In order to use the present results to test the predictions of the geometrical model [17], it would be necessary to convert the measured values of p_L^x to the average fraction of L vacancies produced in the collisions (p_L), which is the quantity that is actually described by the geometrical model. Unfortunately, in the absence of a reliable method for estimating the rates of both intra- and interatomic transitions in multiply ionized atoms, accurate conversion is not possible at the present time. However, it is encouraging to find that the present results for Ar (a target in which interatomic transitions cannot occur) are much closer to the geometrical model predictions than those for solid targets.

For the Ar gas target, further improvement in the agreement between the experimental values of p_L^x and the corresponding theoretical predictions for p_L can be attained by accounting for two other effects that reduce the observed satellite p_L^x values. One is the collisional quenching [12] that reduces the intensity of the $^3P \rightarrow {}^1S$ peak relative to the $^1P \rightarrow {}^1S$ peak and the other is the absence of a $K\alpha L^8$ peak in the x-ray satellite spectrum due to the impossibility of $K\alpha$ x-ray emission in an atom with an empty L shell. The potential impact of the former can be estimated for cases (such as those involving Au, Ta, Ho, Xe, and Kr projectiles) in which the two major $K\alpha L^7$ satellite peak components are resolved. This can be done by replacing the number of counts in the $^3P \rightarrow {}^1S$ peak with that in the $^1P \rightarrow {}^1S$ peak. The magnitude of the latter effect can be estimated from the relative intensities of the $K\beta L^8$ and $K\beta L^7$ satellites or the $K^2\beta L^8$ and $K^2\beta L^7$ hypersatellites for cases in which these peaks are prominent and available (i.e., those involving Ta and Ho projectiles). It was found that the correction for the effect of collisional quenching described above increases the best-fit value of a (for the $K\alpha$ satellites) by about 1%, i.e., to 0.864 ± 0.010, which is somewhat closer to, but still below the best-fit value of 0.909 ± 0.006 obtained from the $K\alpha$ hypersatellites. Adding the estimated (nonexisting) contribution from KL^8 configurations increases the values of p_L^x in the $K\alpha$ satellite (hypersatellite) spectra induced by Ho and Ta projectiles by 5% and 8% (8% and 8%), respectively.

The best-fit logistic curve for p_L^x obtained from the Ar $K\alpha$ hypersatellites is always above the curve obtained from the $K\alpha$ satellites. The difference in their asymptotic values amounts to about 6%. This reflects the fact that an increased degree of K-shell ionization also leads to an increased degree of L-shell ionization. Apparently, the smaller impact parameter collisions that are more likely to result in double K vacancy production are also more effective at removing L electrons.

V. CONCLUSIONS

Spectra of $K\alpha$ x rays emitted from Ar gas atoms at atmospheric pressure under bombardment by 10 MeV/amu heavy ions (atomic number 6–79) were measured in high resolution

using a curved crystal spectrometer. The data analysis showed that the apparent average fractions of L vacancies at the time of $K\alpha$ satellite and hypersatellite x-ray emission are well described by logistic functions of the geometrical model's universal variable X. It was found that the p_L^x values for the monatomic gas Ar are systematically higher than those for solid targets over the whole range of X investigated and exceed a 50% increase at $X > 11$. The cause of this difference is attributed to L-vacancy transfer via interatomic transitions from neighboring atoms in the case of solid targets. On the other hand, the Ar p_L^x values are smaller (by as much as 23%) than the theoretical p_L values predicted by the geometrical

model. It is likely that a substantial portion of this difference is due to intra-atomic postcollision vacancy rearrangement prior to $K\alpha$ x-ray emission. A comparison of the Ar p_L^x values obtained for the $K\alpha$ hypersatellites with those for the satellites revealed that the L-vacancy production probability is enhanced by about 6% in collisions in which both K electrons are removed.

ACKNOWLEDGMENT

[1] R. L. Watson, T. Chiao, and F. E. Jenson, Phys. Rev. Lett. **35**, 254 (1975).

[2] C. F. Moore, D. L. Matthews, and H. H. Wolter, Phys. Lett. **54A**, 407 (1975).

[3] R. L. Kaufman, K. A. Jamison, T. J. Gray, and P. Richard, Phys. Rev. Lett. **36**, 1074 (1976).

[4] F. Hopkins, A. Little, N. Cue, and V. Dutkiewicz, Phys. Rev. Lett. **37**, 1100 (1976).

[5] R. L. Watson, A. K. Leeper, B. I. Sonobe, T. Chiao, and F. E. Jenson, Phys. Rev. A **15**, 914 (1977).

[6] J. A. Demarest and R. L. Watson, Phys. Rev. A **17**, 1302 (1978).

[7] V. Horvat, R. L. Watson, and Y. Peng, Phys. Rev. A **74**, 022718 (2006).

[8] R. D. Deslattes, E. G. Kessler, P. Indelicato, L. de Billy, E. Lindroth, and J. Anton, Rev. Mod. Phys. **75**, 35 (2003).

[9] J. L. Campbell and T. Papp, At. Data Nucl. Data Tables **77**, 1 (2001).

[10] R. L. Watson, J. M. Blackadar, and V. Horvat, Phys. Rev. A

60, 2959 (1999).

[11] V. Horvat and R. L. Watson, J. Phys. B **34**, 777 (2001).

[12] R. L. Watson, J. Pálinkás, G. J. Pedrazzini, B. Bandong, C. Can, D. A. Church, and R. A. Kenefick, Phys. Rev. A **35**, 1510 (1987).

[13] M. H. Chen, B. Crasemann, and H. Mark, Phys. Rev. A **25**, 391 (1982).

[14] G. Schiwietz and P. L. Grande, Nucl. Instrum. Methods Phys. Res. B **175**, 125 (2001).

[15] J. P. Desclaux, Comput. Phys. Commun. **9**, 31 (1975).

[16] V. Horvat, R. L. Watson, and J. M. Blackadar, Phys. Rev. A **77**, 032724 (2008).

[17] B. Sulik, I. Kadar, S. Ricz, D. Varga, J. Vegh, G. Hock, and D. Berenyi, Nucl. Instrum. Methods Phys. Res. B **28**, 509 (1987).

[18] J. H. McGuire and P. Richard, Phys. Rev. A **8**, 1374 (1973).

[19] V. Horvat, R. L. Watson, and J. M. Blackadar, Nucl. Instrum. Methods Phys. Res. B **170**, 336 (2000).

[20] R. L. Watson, V. Horvat, and Y. Peng, Phys. Rev. A **78**, 062702 (2008).